Indian Journal of Biochemistry & Biophysics
Vol. 63, August 2026, pp. 947-957
DOI: 10.56042/ijbb.v63i8.21869

Virtual screening of anthranilic acid-based alkaloids from *Persicaria tinctoria* as inhibitors of acetylcholinesterase

Nischal Saxena* and Rajesh Shukla
Faculty of Pharmaceutical Sciences, Manglayatan University, Jabalpur-483 001, Madhya Pradesh, India

Received 22 July 2025; *revised 06 May 2026*

Alzheimer's disease (AD) is a progressive neurodegenerative disorder characterized by memory loss and cognitive decline, often linked to the dysfunction of acetylcholinesterase (AChE). In this study, anthranilic acid-based alkaloids isolated from *Persicaria tinctoria* were virtually screened for their inhibitory potential against AChE using molecular docking and molecular dynamics simulations. Docking analysis revealed that several compounds exhibited strong binding affinities, interacting with key residues at the catalytic active site, peripheral anionic site, and choline-binding site. Among them, Compound 13 demonstrated the highest binding affinity (–9.01 kcal/mol) and a favorable inhibition constant (253.32 nM), forming stable interactions with critical residues including TRP86, TYR124, TYR341, and PHE295. Molecular dynamics simulations confirmed the structural stability and flexibility of the AChE–Compound 13 complex, further supporting its potential as a lead candidate. Other compounds also showed varied inhibitory profiles, targeting peripheral and allosteric sites of the enzyme. These findings suggest that alkaloids from *P. tinctoria* may serve as promising natural scaffolds for developing novel AChE inhibitors for AD therapy.

Keywords: Acetylcholinesterase, Alzheimer's disease, Anthranilic acid-based alkaloids, Natural inhibitors, *Persicaria tinctoria*, Radius of gyration (Rg)

Alzheimer's disease is a serious neurological condition that mainly affects memory and thinking abilities, significantly impacting a person's quality of life. It involves the gradual breakdown of brain cells, leading to symptoms such as forgetfulness, difficulty in reasoning, and noticeable behavioral changes. In its early stages, people may struggle to recall recent events, names, or conversations[1]. As the condition progresses, they may become confused, have trouble speaking or understanding language, and find problem-solving increasingly difficult. Mood changes, social withdrawal, and neglect of personal care are also common[2]. In advanced stages, individuals often lose the ability to perform everyday tasks or recognize familiar people. The disease is marked by the buildup of beta-amyloid protein clumps and twisted tau proteins in the brain. Although the precise cause is not fully understood, advancing age, genetic makeup, and certain lifestyle habits are known risk factors[3].

Although current anti-Alzheimer's medications can help ease symptoms and temporarily slow down memory loss, they have certain limitations. Common side effects include digestive discomfort, trouble sleeping, and tiredness[4]. The effectiveness of these drugs also varies from person to person, and in some cases, the benefits may be minimal. Over time, the body may become less responsive to the medication, reducing its effectiveness. Moreover, these treatments do not target the root causes of Alzheimer's disease, highlighting the need for continued research to find more precise and long-lasting treatments. Nature remains an important source of medical compounds, offering a wide range of biologically active substances[5–7]. Many drugs used today, such as antibiotics, painkillers, and cancer treatments, were originally discovered in plants, marine life, and microbes. These natural compounds often have unique chemical structures that can lead to effective and innovative therapies for many health conditions.

Plants have become valuable sources of therapeutic agents, aiding in the treatment of various conditions like CNS disorders, diabetes, and cancer. Plant-derived compounds possess bioactive properties that can influence neurological activity, control blood sugar levels, and show promise in cancer therapy. These natural substances have gained attention for their potential to address a wide range of health issues, offering alternative or complementary options

*Correspondence:
E-mail: saxena1nischal@gmail.com

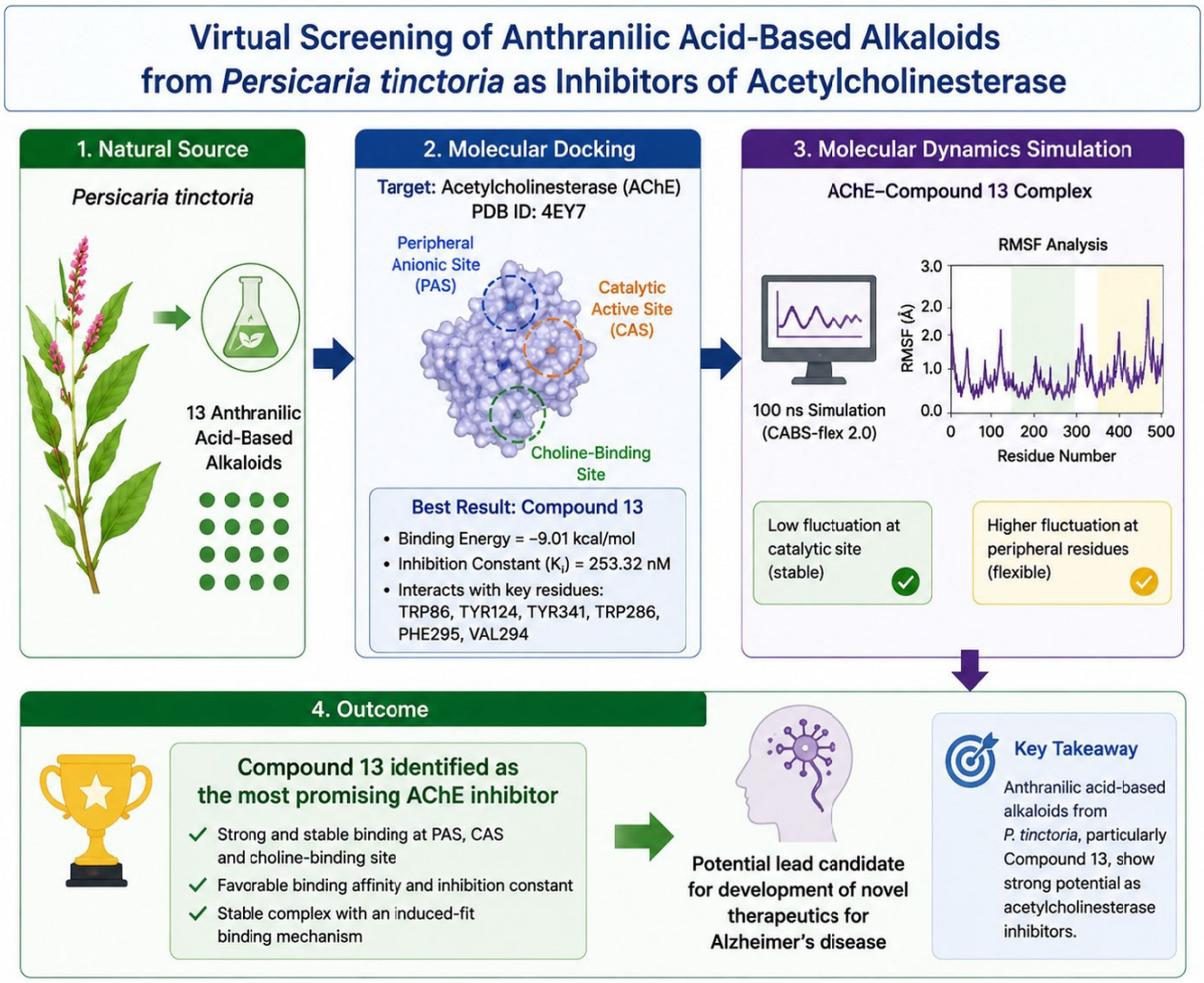

Graphical abstract

to conventional treatments. *Persicaria tinctoria*, a commercially valuable plant, is the primary source of natural indigo dye and the bioactive metabolite indirubin. Several undescribed anthranilic acid-based alkaloids and natural products, along with known compounds, have been isolated from its leaves using advanced techniques[8]. The aim of present work was to perform virtual screening of these compounds and acetylcholinesterase inhibitors.

Materials and Methods

Molecular docking

The software tools used in this study included Python 2.7, which was downloaded from www.python.com, MGL Tools from the Molecular Graphics Laboratory, and AutoDock 4.2, acquired from www.scripps.edu. Discovery Studio Visualizer 4.1 was sourced from www.accelerys.com. Python 2.7 served as the primary platform for the molecular docking experiments. The study focused on *Persicaria tinctoria* alkaloids with acetylcholinesterase (PDB ID: 4EY7) obtained from the Protein Data Bank (PDB) at www.rcsb.org/pdb. Pre-docking steps included editing the acetylcholinesterase structures, removing heteroatoms, and adding C-terminal oxygen. The A chain of 4EY7 was taken out of the Protein Data Bank and chosen to be used in the studies of molecular docking. Any other chains, co-crystallized ligands, and non-essential heteroatoms were eliminated, and crystallographic water molecules were removed other than those being part of an active-site critical interaction. Missing residues and atoms were detected and fixed and hydrogen atoms were added to the structure to indicate physiological conditions. Proper bond orders and protonation states were assigned especially to catalytically important residues. Minimizing energy of the prepared protein structure was

done by minimizing energy using an appropriate force field to reduce steric clashes and optimize geometry. Partial atomic charges were calculated and the final structure was changed to a docking compatible format to be used in future virtual screening studies. Ligands were assigned Gasteiger-Marsili partial charges, non-polar hydrogen atoms were merged, and torsions were allowed during docking[9]. Active binding pockets were identified using LigPlot, and the Computed Atlas of Surface Topography of Proteins (CASTp) server was used to validate these pockets. A docking grid was generated using AutoDock Tools to define the active binding region of the target protein prior to docking simulations performed with AutoDock Vina. The grid box was centered at coordinates X = −14.036, Y = −43.102, and Z = 28.966 with dimensions of 72 × 52 × 60 grid points along the x, y, and z axes, respectively. A grid spacing of 0.375 Å was applied, resulting in a total of 236,009 grid points covering the binding pocket. Docking simulations employed the Lamarckian Genetic Algorithm with default energy minimization settings, and Discovery Studio was used for visualizing the docking results (Table 1).

Redocking and RMSD calculation

The crystallographic ligand was extracted from the protein–ligand complex obtained from the Protein Data Bank and used for redocking validation. Molecular docking was performed using AutoDock Vina by defining the grid box around the original binding site of theco-crystallized ligand. The docked pose was compared with the experimentally determined ligand conformation by calculating the root mean square deviation (RMSD) between the heavy atoms of both structures. RMSD calculation and structural alignment were performed using a Python-based script implemented in Google Colaboratory to assess the reliability of the docking protocol.

Molecular dynamics

Compound 13 complexed with acetylcholinesterase (PDB ID: 4EY7) was simulated by using Cresset Flare and OpenMM simulation platform. The default protein-ligand force field parameters that are included in Flare were used to prepare the system. The solvation of the complex was done in an explicit model of water with a cubic periodic box with a padding distance of 10 A and the necessary counterions were added to neutralize the system. Minimization of energy was then done followed by equilibration at the standard conditions. An ensemble of production of 10 ns was conducted under NPT conditions. Root mean square deviation (RMSD), root mean square fluctuation (RMSF), radius of gyration (Rg), standard deviation amongst conformational clusters, and average distance to cluster centroids were used as post-simulation analyses of structural stability and dynamic behavior of protein -ligand complex.

Table 1 — Docking interaction of *Persicaria tinctoria* compounds with with 4EY7

Compound	Binding Energy (kCal/mol)	Inhibition constant	Type of Interaction	Interacting residues
1a	-8.28	857.61 Nm	Van der Waals	TYR (A:124), PHE (A:295), PHE (A:297), PHE (A:338), TYR (A:337), TYR (A:341), GLU (A:202), GLY (A:120), TRP (A:236)
			Conventional Hydrogen Bond	SER (A:203), GLY (A:121), GLY (A:122), ALA (A:204)
			π-Lone Pair Interaction	HIS (A:447)
			π-Alkyl Interaction	TRP (A:86)
1b	-7.6	2.67 µm	Van der Waals	TRP (A:286), PHE (A:297), HIS (A:447), GLY (A:121), THR (A:83), ASN (A:87)
			Conventional Hydrogen Bond	SER (A:125)
			Carbon Hydrogen Bond	ASP (A:74)
			π-Sigma Interaction	TRP (A:86)
			π-π Stacked Interaction	TYR (A:124)
			π-π T-shaped Interaction	TYR (A:341)
			π-Alkyl Interaction	TYR (A:337), PHE (A:338)
2	-6.8	10.37 µm	Van der Waals	LEU (A:289), TRP (A:286), PHE (A:295), SER (A:293)
			Conventional Hydrogen Bond	ARG (A:296)
			π-Alkyl Interaction	VAL (A:294), PHE (A:297), PHE (A:338), TYR (A:341)

(*Contd.*)

Table 1 — Docking interaction of *Persicaria tinctoria* compounds with with 4EY7 (*Contd.*)

Compound	Binding Energy (kCal/mol)	Inhibition constant	Type of Interaction	Interacting residues
3	-7.4	33.76 µm	Van der Waals	TRP (A:286), PHE (A:297), PHE (A:295), TYR (A:341)
			Conventional Hydrogen Bond	TYR (A:124)
			Carbon Hydrogen Bond	PHE (A:295)
			π-Donor Hydrogen Bond	PHE (A:338)
			π-π Stacked Interaction	TYR (A:337)
			π-π T-shaped Interaction	PHE (A:338)
			π-Alkyl Interaction	VAL (A:294), PHE (A:338), TYR (A:337)
4	-7.73	2.17 µm	Van der Waals	TRP (A:286), PHE (A:297), PHE (A:295), LEU (A:289), SER (A:293), PHE (A:338)
			Conventional Hydrogen Bond	TYR (A:124)
			Carbon Hydrogen Bond	ARG (A:296)
			π-π Stacked Interaction	TYR (A:337)
			π-π T-shaped Interaction	TYR (A:341)
			Alkyl Interaction	VAL (A:294)
			π-Alkyl Interaction	PHE (A:338), TYR (A:337)
5	-7.15	5.76 µm	Van der Waals	TYR (A:341), PHE (A:297), TYR (A:124), HIS (A:447)
			Conventional Hydrogen Bond	ARG (A:296)
			Carbon Hydrogen Bond	SER (A:293)
			Pi-Pi Stacked	PHE (A:338)
			Pi-Pi T-shaped	TYR (A:337)
			Alkyl	VAL (A:294), TRP (A:286)
			Pi-Alkyl	PHE (A:338), TYR (A:337)
6	-6.71	12.15 µm	Van der Waals	TYR (A:72), ASN (A:87), VAL (A:73), GLY (A:121), HIS (A:447), TRP (A:439)
			Conventional Hydrogen Bond	TYR (A:124), TYR (A:337), TYR (A:341), THR (A:83), ASP (A:74)
			Pi-Pi Stacked	TRP (A:86)
			Alkyl	PRO (A:88)
7	-7.05	6.81 µm	Van der Waals	GLN (A:71), ASN (A:87), VAL (A:73), GLY (A:121), HIS (A:447), SER (A:125)
			Conventional Hydrogen Bond	TYR (A:337), TYR (A:341), THR (A:83), ASP (A:74)
			Pi-Pi Stacked	TRP (A:86)
			Alkyl	PRO (A:88)
			Pi-Alkyl	TYR (A:72), TYR (A:124)
8	-8.65	458.01 Nm	van der Waals	GLY A:121, HIS A:447, SER A:125, ASN A:87, GLN A:71, VAL A:73
			Conventional Hydrogen Bond	ASP A:74, TYR A:337, TYR A:341
			Pi-Pi Stacked	TRP A:86
			Alkyl	PRO A:88, TYR A:72, TYR A:124
			Pi-Alkyl	TRP A:86
9	-7.92	1.56 µm	van der Waals	GLY A:121, HIS A:447, SER A:125, ASN A:87, GLY A:448, ASP A:74, THR A:83
			Conventional Hydrogen Bond	TYR A:124, TYR A:337, TYR A:341
			Pi-Pi Stacked	PHE A:338
10	-8.57	521.78 Nm	van der Waals	LEU A:289, SER A:293, PHE A:297, TYR A:124, TYR A:337
			Conventional Hydrogen Bond	ARG A:296
			Pi-Sigma	VAL A:294
			Pi-Pi Stacked	TYR A:341, PHE A:338
			Pi-Pi T-shaped	TRP A:286, PHE A:295
11	-8.31	812.59 Nm	van der Waals	LEU A:289, SER A:293, VAL A:294, TRP A:286, PHE A:295, PHE A:297, TYR A:124, TYR A:341
			Conventional Hydrogen Bond	ARG A:296
			Pi-Pi Stacked	PHE A:338

(*Contd.*)

Table 1 — Docking interaction of *Persicaria tinctoria* compounds with with 4EY7 (*Contd.*)

Compound	Binding Energy (kCal/mol)	Inhibition constant	Type of Interaction	Interacting residues
12	-6.52	16.75 µm	van der Waals	LEU A:289, PHE A:297, TYR A:124
			Conventional Hydrogen Bond	SER A:293, ARG A:296, VAL A:294, PHE A:295
			Carbon Hydrogen Bond	PHE A:295
			Pi-Alkyl	TRP A:286, PHE A:338, TYR A:341
13	-9.01	253.32 Nm	van der Waals	LEU A:289, SER A:293, PHE A:297, TYR A:124
			Conventional Hydrogen Bond	ARG A:296, PHE A:295
			Pi-Sigma	VAL A:294
			Pi-Pi T-shaped	TYR A:337, TRP A:286
			Pi-Alkyl	TYR A:72, TYR A:341, PHE A:338

Results

Molecular docking

In this study, a series of compounds were evaluated for their inhibitory interactions with acetylcholinesterase (AChE). Multiple non-covalent interactions were found to stabilize the binding of Donepezil with the A chain of 4EY7 and aromatic residues, TRP86, TYR337, and PHE338, were observed to form π- -stacking interactions that led to the robust anchoring of the ligand in the active-site gorge. Hydrogen bonding was achieved with residues such as ARG296 and SER293, and binding specificity was increased. Further van der Waals and hydrophobic contacts were established with residues like VAL294, PHE295, and LEU289, which assist in stabilizing ligands. Also, the interaction with the peripheral anionic site residues, such as TYR341 and TRP286, were facilitated, which demonstrated effective dual-site binding in the enzyme. Compound 1a was bound extensively to the Catalytic Active Site (CAS) and the Oxyanion Hole, with hydrogen bonds formed with Ser203, Gly121, Gly122, and Ala204, while Pi-alkyl interactions were observed with Trp86, suggesting effective CAS occupancy. Compound 1b was stabilized at the Peripheral Anionic Site (PAS) via hydrogen bonding with Ser125 and carbon hydrogen bonding with Asp74. Binding to PAS through pi-stacking with Tyr124 and Tyr341 was also observed. Compound 2 was anchored within the Acyl Pocket and Gorge Entrance, without engagement of catalytic triad residues, indicating allosteric inhibition. Compound 3 was situated at PAS and the Acyl Pocket through van der Waals and pi-π stacking interactions, implying moderate, reversible inhibition. Similarly, Compounds 4 and 5 were bound at PAS, with Compound 4 predicted as a competitive inhibitor and Compound 5 as a non-competitive allosteric modulator. Compounds 6–13 were also found to interact predominantly with PAS, some extending into the CAS or Choline Binding Site. Multiple hydrogen bonding, van der Waals, and pi interactions were detected, and inhibitory mechanisms were predicted as competitive, non-competitive, or mixed, based on binding regions and residue engagement. Compound 13 was identified as the most promising acetylcholinesterase (AChE) inhibitor. It exhibited strong and extensive interactions at the Peripheral Anionic Site (PAS), engaging key residues such as Tyr72, Tyr341, Trp286, and Phe338 through multiple pi-T-shaped and van der Waals interactions. Although it did not directly bind to the Catalytic Active Site (CAS), its strong PAS engagement suggested a powerful allosteric inhibitory mechanism, effectively preventing substrate entry and alignment.

Redocking and RMSD

To validate the reliability of the docking procedure, the co-crystallized ligand was re-docked into the active site of the target protein using AutoDock Vina. The docking grid was centered on the original ligand binding pocket to ensure that the redocking experiment reproduced the experimentally determined binding environment. Following docking, the predicted ligand conformation was superimposed onto the crystallographic ligand extracted from the Protein Data Bank structure. The structural similarity between the docked and experimental ligand poses was evaluated by calculating the root mean square deviation (RMSD) between the heavy atoms of both structures. The calculated RMSD value was 1.888 Å, indicating a strong agreement between the docked and crystallographic conformations. Visual inspection of the superimposed structures confirmed that the redocked ligand occupied the same binding pocket and maintained a similar orientation as observed in the crystal structure. These findings demonstrate that the docking protocol accurately reproduces the

experimental binding mode of the ligand within the active site.

Molecular dynamics

RMSD

RMSD To assess the stability of protein structure 4EY7 in the apo form and when it is complexed with Compound 13 in the chosen molecular dynamics simulation, the root mean square deviation (RMSD) analysis was conducted in order to determine the structural stability of the protein structure in the apo form and with Compound 13. The RMSD curve of the apo protein (4EY7) indicates that there is an initial increase in the apo protein between the range of about 0.6 A to about 1.3 A in the first nanosecond, which means that the system equilibrates very fast (Fig. 1). Following this early relaxation, the values of RMSD vary within a rather stable range of 1.317 A during the rest of the 10 ns simulation indicating that the protein backbone is well equilibrated and stable. Conversely, there is an increase in the deviation of the RMSD profile of the 4EY7-Compound 13 complex than the apo structure. The RMSD rises quickly in the beginning of the simulation and reaches a level of 3.0-3.5A. Although the values of the RMSD are larger, the trajectory has a steady variation on the average without any sudden spikes, which means that the complex is in a stable conformational state once the initial equilibration period has passed. RMSD plateau of the protein-ligand complex at around 1 ns indicates that the protein-ligand complex is structurally stable at the time of simulation. In general, the RMSD results show equilibrium of both systems but the ligand-bound system.

RMSF

To analyse the flexibility of the 4EY7 protein at the residue-level during the molecular dynamics simulation, the root mean square fluctuation (RMSF) analysis was conducted to study the flexibility of the protein in its apo form and in complex with Compound 13. RMSFD values of every amino acid residue were determined to determine the times of structural flexibility and stability in the protein. The apo 4EY7 form had relatively low values of RMSF at most of the residues and tended to range between about 1.0 to 2.5 A. These findings suggest that most of the residues were structurally rigid in the course of the simulation. Minor peaks at a few positions are loop regions which tend to be more flexible than the structured secondary elements like α-helices and β-sheets. Conversely, the 4EY7- Compound 13 complex showed relatively a higher value of RMSF during protein sequence. Some of the residues exhibited changes in the range of 2.05.0 A, indicating that more local mobility occurs on binding of the ligand. (Fig. 2) It is important to note that there were strong peaks towards the C-terminal part, especially around the residues around the positions 490-520 as the RMSF values were significantly higher. Such high variability is probably related to flexible loop or terminal loops which are dynamic in nature.On

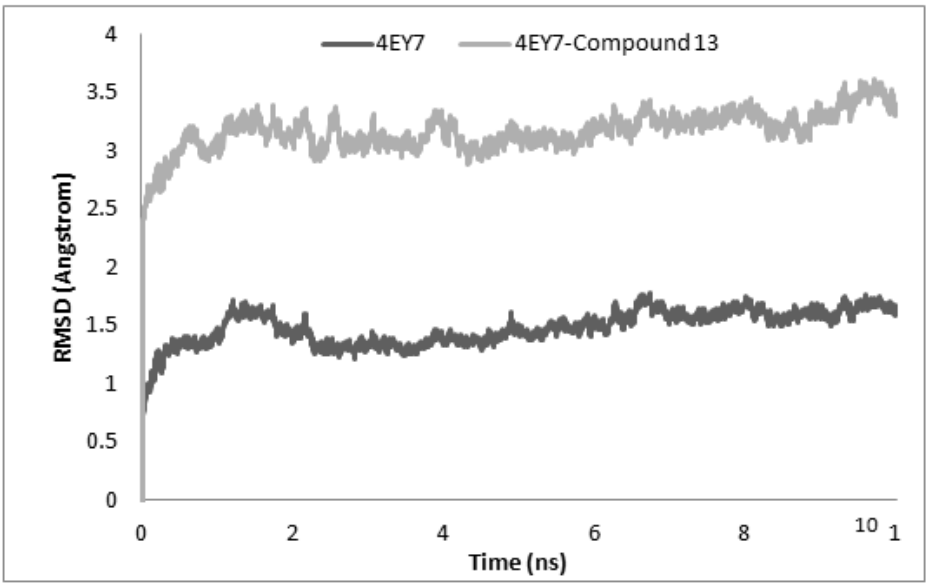

Fig. 1 — Root mean square deviation analysis of the backbone atoms of protein 4EY7 and the 4EY7–Compound 13 complex during a 10 ns molecular dynamics simulation

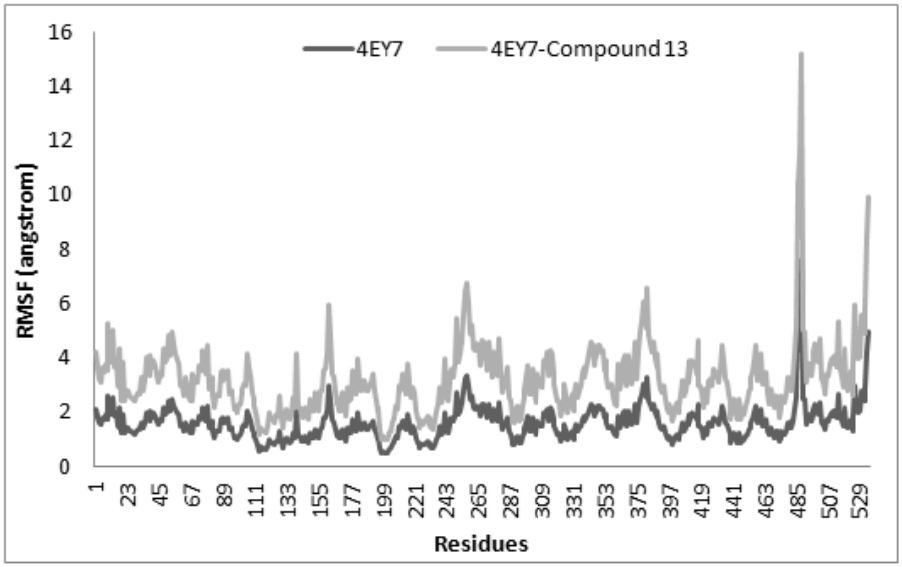

Fig. 2 — Root mean square fluctuation profile of amino acid residues of 4EY7 in the apo form and in complex with Compound 13 during the molecular dynamics simulation

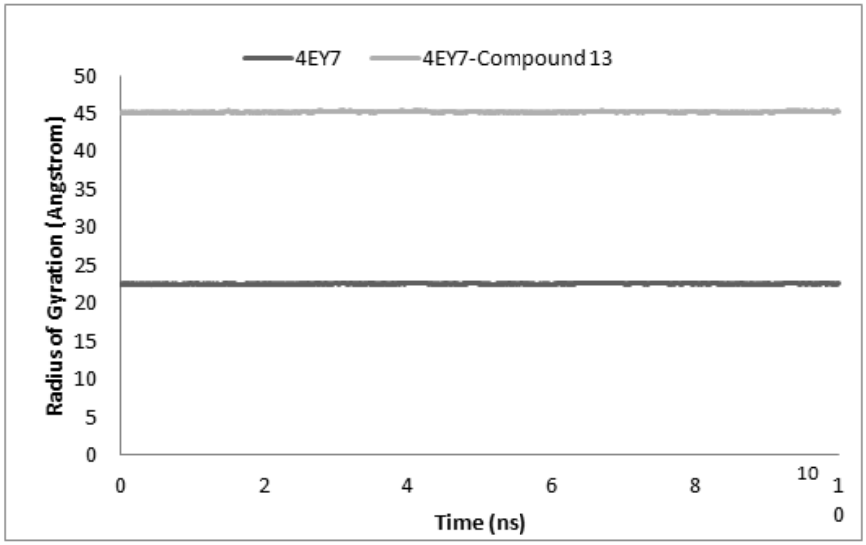

Fig. 3 — Radius of gyration profiles of 4EY7 and the 4EY7–Compound 13 complex over a 10 ns molecular dynamics simulation

the whole, the RMSF analysis shows that, although the ligand binding precondition the slight increase in local flexibility of particular parts of the protein, the most residues preserve their stable forms during the simulation, which proves the integrity of the structure of the 4EY7 9 Compound 13 complex.

Radius of Gyration

The profiles of the radius of gyration (Rg) of the unbound protein (4EY7) and the 4EY7-Compound 13 complex were measured during a 10 ns simulation to assess the compactness and stability of the structure over the whole length of the protein. The trajectories indicate that the two systems quickly reach equilibrium and that the values of Rg in both systems remain more or less the same during the simulation time frame. The apo protein has an average Rg of about 22–23 A which means that it is a compact and stable fold with few fluctuations. In the same fashion, the protein-ligand complex has a constant Rg profile, the values being nearly similar to those of the unbound system. The changes in the two systems are slight (less than 0.5 A) indicating that there were no major expansion or contraction events in the course of the simulation (Fig. 3) Notably, the fact that the Rg traces do not show any systematic drift or sudden deviations would suggest that none of the systems experiences an unfolding process or significant conformational rearrangements. The more

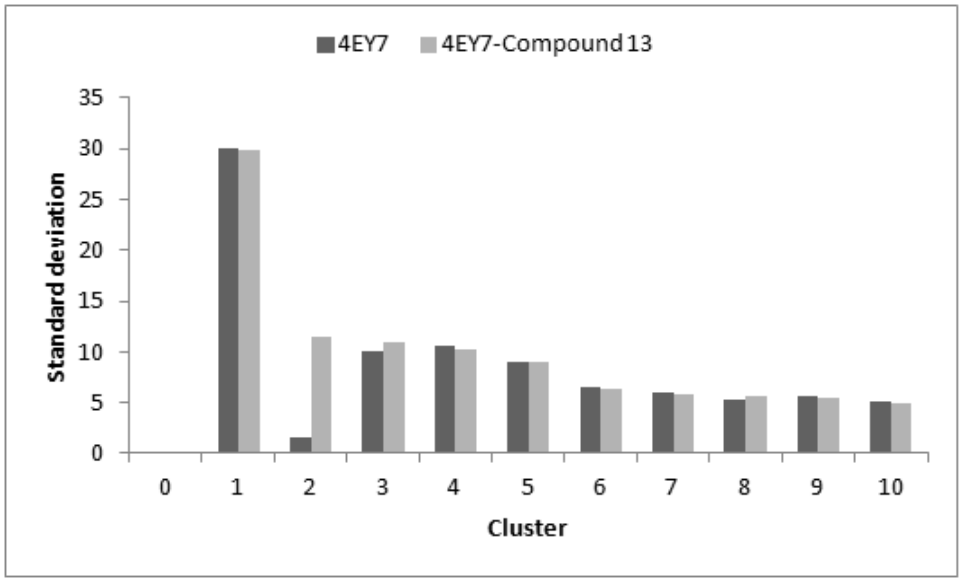

Fig. 4 — Cluster-wise standard deviation (SD) comparison of 4EY7 and the 4EY7–Compound 13 complex

complicated form has a slightly smoother curve, suggesting that there is a slight stabilization when the ligand is bound, but the variation is not significant. In general, the Rg analysis shows that Compound 13 binding does not interfere with the overall structure of 4EY7. Rather, both systems maintain an unperturbed and stable conformation throughout the simulation.

Standard Deviation among clusters

The distribution of standard deviation (SD) of the clusters of both the unbound protein (4EY7) and the 4EY7-Compound 13 complex shows that there are different patterns of structural variability. Cluster 1 has the largest SD values of both systems at about 30 meaning that there is a large conformational variance in this cluster. Clusters 2-10, on the other hand, have significantly smaller SD values, with an average of about 1-11, indicating tighter and homogeneous conformational groupings. It is important to note that, there is a strong difference between the apo and complex systems in cluster 2. Although the unbound protein has a very low SD (~1-2), the complex has a much higher SD (~11-12) meaning that there is more structural variability with the ligand binding in this particular cluster. In clusters 3 and 4, the two systems exhibit moderate SD values (around 1011), and the two systems exhibit slight variations, indicating similar conformational spread. Starting with cluster 5, SD values of both systems slowly decrease and approach each other with the range of values normally being between 5 and 9. This tendency implies the growing structural homogeneity of these clusters (Fig. 4). These later clusters also have not shown much in the difference between the apo and ligand-bound forms, suggesting that there is not a significant change in conformational variability in these states due to ligand binding. In general, the findings reveal that although the majority of the clusters are characterized by similar dispersion of the structure between the two systems, some clusters (especially cluster 2) demonstrate greater variability in the presence of Compound 13.

Mean distance to centroid

The average centroid distance is a valuable measure that can be used to measure the compactness and internal similarity of structures in a cluster. The small set of values measured in all clusters of 4EY7 (and the complex of 4EY7 with Compound 13) indicates that the clustering process has been able to capture well-defined and structurally coherent conformational states. This implies that there is no domination of the conformational states of the molecular dynamics trajectories but rather they explore a comparatively stable conformational landscape. This high similarity between the apo and ligand-bound systems also suggests that binding of ligands does not cause causes of perturbation of the protein at the global level to a significant extent. This finding is in line with the previous reviews such as the results of radius of gyration and standard deviation which also showed the structural stability and low variability. The slight changes in centroid distance in some clusters (*e.g.* cluster 2 and 8) can be due to some

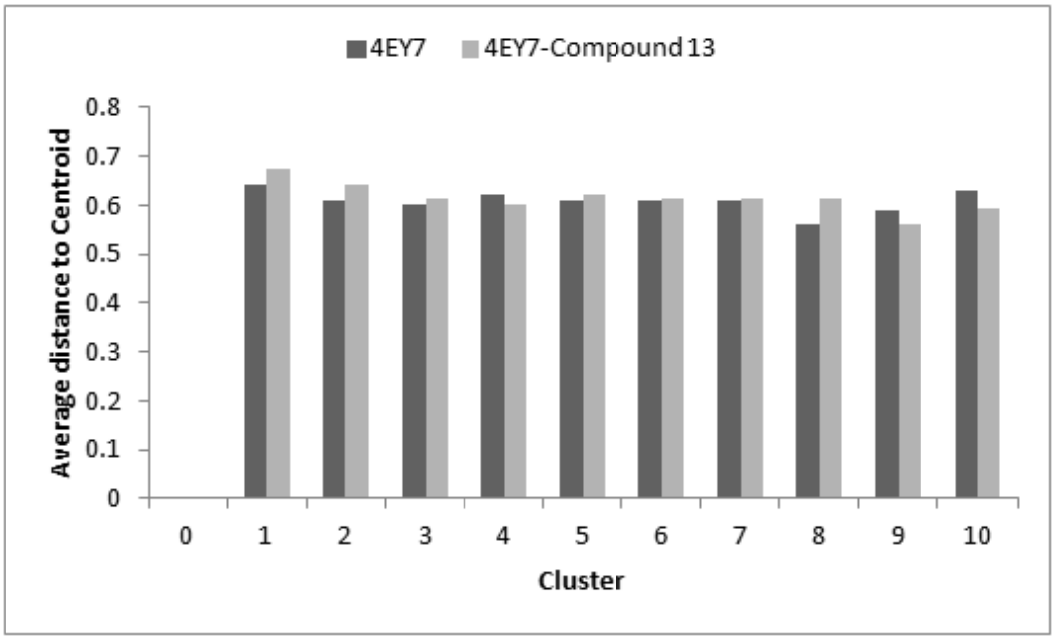

Fig. 5 — Average distance to centroid comparison of 4EY7 and the 4EY7–Compound 13 complex

local flexibility that has been added by the ligand, maybe in or close to the binding site (Fig. 5). Notably, the lack of big centroid distances indicates that there is no cluster that is an outlier or one that is highly disordered. This supports the idea that the two systems will continue to be structurally stable during the simulation. The consistency between the trend of centroid distance and standard deviation also demonstrates the validity of the clustering method as an effective way of representing statistically significant differences in conformations. All of this indicates that Compound 13 does not interfere with the inherent conformational arrangement of 4EY7.

Discussion

Persicaria tinctoria, commonly known as Chinese indigo, is a medicinal plant traditionally valued for its dye-producing and therapeutic properties. Recent phytochemical investigations have revealed the presence of several bioactive compounds, including anthranilic acid-based alkaloids, which may hold pharmacological significance. The therapeutic potential of this plant has been explored in various disease models, highlighting its antioxidant, anti-inflammatory, and neuroprotective effects. In the present study, virtual screening of these alkaloids was conducted to evaluate their inhibitory potential against acetylcholinesterase, a key enzyme in Alzheimer's disease pathology.

Compound 13 emerged as the most promising inhibitor of acetylcholinesterase (AChE), displaying the lowest binding energy of –9.01 kcal/mol and an inhibition constant of 253.32 nM among all tested compounds. Its strong and specific interactions with critical AChE residues contributed to its superior binding affinity and inhibitory potential. It engaged the catalytic site residue TRP86 through π-alkyl interactions, enhancing ligand affinity at the choline-binding site. Moreover, significant interactions were observed with peripheral anionic site (PAS) residues, including TYR124, TYR341, and TRP286, which are essential for ligand recognition and allosteric modulation. Interactions with oxyanion hole residues PHE295 and VAL294 further stabilized the transition state during enzymatic inhibition. The compound also formed contacts with LEU289, PHE297, and SER293 near the gorge entrance, suggesting deep penetration and secure binding within the active-site gorge, justifying its selection for molecular dynamics (MD) simulations. In comparison, Compound 1a showed extensive interactions with CAS residues (S203, H447), oxyanion hole residues (G121, G122, A204), and choline-binding site residues (W86), contributing to strong inhibition. Compounds 1b, 3, 5, and 10 also exhibited significant inhibitory effects by forming stable hydrogen bonds, π-π stacking, and van der Waals interactions with key residues such as TYR124, F295, F338, and D74. However, Compound 13's broader interaction profile and deeper active site engagement established it as the most effective AChE inhibitor.

RMSD is an important parameter that is used to measure the conformational stability of protein structures in molecular dynamics simulations. In the current analysis, 4EY7 in its apo form exhibits comparatively small changes in RMSD during the simulation pathway and this result reveals stable backbone conformation. The fact that the values of RMSD stabilized following the initial equilibration period indicates that the protein is in its usual state in the context of the simulation. The 4EY7-Compound 13 complex has increased values of RMSD as compared to the apo structure. This rise in RMSD could be due to conformational changes in the protein structure due to the binding of the ligand. The structural rearrangements that occur during molecular dynamics simulations are usually induced by the presence of a ligand as the protein changes to fit the ligand into the binding pocket. Notably, despite the increase in the RMSD values, there are no significant fluctuations or sudden deviations, which means that the protein-ligand complex is structurally stable throughout the simulation. The plateau that occurred later than the initial simulation period indicates that the system attains equilibrium and is in a steady conformational state. This action would suggest that Compound 13 obtains a stable connection with the binding site of 4EY7, whereas it displays a moderate level of flexibility in the protein structure. This elasticity could be useful in ensuring stable interactions in the binding pocket. In general, the RMSD values confirm that the 4EY7-Compound 13 complex was stable within the period of the simulations.

RMSFD analysis is used to gain extensive information about the dynamic behavior of individual amino acid residues during a molecular dynamics simulation. In the analysis, the apo conformation of the 4EY7 protein exhibited a comparatively low extent of residue variations, which demonstrates that the protein backbone is fairly stable in its conformation when simulated. The minor peaks found at some residues are typical of flexible loop sequences or solvent-exposed sequences which have a natural higher mobility than structured domains. The 4EY7-Compound 13 complex had slightly increased values of RMSF at various residues than in apo structure. This flexibility can be explained by changes in the conformational changes that can be detected when a ligand is bound. The surrounding residues can slightly rearrange when a ligand binds to the active site or binding pocket to maximize binding interactions (hydrogen bonding, hydrophobic contacts, and electrostatic interactions). The largest changes were noticed around the C-terminal residues, where RMSF values were significantly elevated. Protein terminal regions can be very flexible and do not necessarily take part in ligand binding, hence extra changes in these regions do not tend to affect the overall stability of the protein-ligand complex. Notably, residues in the central parts of the protein had comparatively constant RMSF values, indicating that the overall structural structure of the protein was retained throughout the simulation. These results point to the fact that Compound 13 does not disrupt the protein structure and establishes a stable complex with 4EY7.

The profiles of stability of the radius of gyration of the apo and ligand-bound 4EY7 are significant because they give a clue of the structural implications of ligand binding. Rg is an important measure of protein compactness and the values that are seen to be constant here point to the fact that the overall folding and tertiary structure is not lost during the simulation. This is especially important since the binding of ligands may occasionally cause a conformational change that stabilises or destabilises the protein structure. Here, the fact that the apo and complex trajectories are similar shows that Compound 13 does not have a significant effect on the overall structure of the protein. The minor decreases in the complex may indicate local stabilization, which might be associated with desirable interactions like hydrogen bonding, hydrophobic contacts, or van der Waals interaction in the binding pocket. But as the average values of Rg are almost the same, these stabilizing effects cannot be attributed to the whole world but only to certain areas. The fact that there is no structural growth or greater flexibility implies that the ligand lacks the strain or destabilizing force on the protein structure. This is a positive sign of binding compatibility and could be associated with binding affinity stability. Also, the Rg values are the same suggesting that the simulation has come to equilibrium and the observed behavior is of a stable system. Combined, the data indicate that Compound 13 could be used as a structurally stable complex with 4EY7 without destabilizing its overall fold, which contributes to the fact that it is a possible successful ligand.

Cluster-wise standard deviation analysis gives a more profound understanding of the conformational heterogeneity of 4EY7 and its complex with Compound 13. Standard deviation is used to quantify the spread of structures in every cluster with larger values implying more variety in conformations. The very large SD of cluster 1 of both systems indicates that the cluster is a highly flexible or transitional

conformational form, which may include a large range of structures sampled in the simulation. Of special interest is the significant growth of SD in cluster 2 in the ligand bound system over the apo form. This suggests that Compound 13 can stabilize or stabilize more than one conformational substates in this cluster, which could increase local flexibility or allow other structural configurations. It can be related to induced-fit mechanisms or dynamic adaptation in the binding-site region. Conversely, the fact that the SD values in most other clusters are similar means that ligand binding does not universally promote structural disorder. Rather, the protein is mostly able to retain its conformational integrity but variability is localized in a number of regions or states. The progressive decrease in SD values between clusters 5-10 also lends evidence to the fact that more well-defined and stable conformational states exist in both systems. These results correspond to the radius of gyration results that revealed a general structural stability. They all imply that Compound 13 does not destabilize the protein but can have a subtle effect on its conformational landscape in a cluster-dependent way. This flexibility in local conformational detail may be significant to functional dynamics or ligand accommodation, supporting the possibility of relevance of Compound 13 as a stabilizing binding partner.

Conclusion

Conclusively, the current research paper reveals that anthranilic acids based alkaloids of *Persicaria tinctoria* have the potential of being effective acetylcholinesterase inhibitors. Compound 13 was identified as the best compound amongst the screened compounds based on its binding affinity and inhibitory potential as indicated by its lowest binding energy and good interactions with key catalytic, peripheral anionic, and oxyanion hole residues. The various functional areas that it can access in the active-site gorge shows that it has an efficient and stable binding mode, rendering it a good candidate of further research. The stability and compatibility of the 4EY7 -Compound 13 complex was further confirmed by the use of molecular dynamics simulations. RMSD and RMSF analysis proved that binding of the ligands only resulted in moderate and localized changes in flexibility without causing structural damage to the whole protein. Radius of gyration and clustering further validated these results and showed that there was persistence of compactness and a constant conformational landscape during the simulation. Small changes in the particular clusters indicate that they can be flexible to conformational changes, which can be useful in accommodating ligands. Overall, Compound 13 exhibits a favorable balance between structural stability and dynamic adaptability, essential for efficient enzyme inhibition. These findings provide a strong computational basis for its potential development as a lead candidate in Alzheimer's disease therapeutics, warranting further experimental validation and optimization.

Acknowledgement

Authors are thankful to Dean, Department of pharmacy, Faculty of Pharmaceutical Science, Mangalaytan University Barela, Jabalpur for providing necessary facilities during the studies.

Conflict of interest

All authors declare no conflict of interest.

References

1 Uwishema O, Mahmoud A, Sun J, Correia IFS, Bejjani N, Alwan M, Nicholas A, Oluyemisi A & Dost B, Is Alzheimer's disease an infectious neurological disease? A review of the literature. *Brain Behav*, 12 (2022) e2728.

2 Drinkwater E, Davies C & Spires-Jones TL, Potential neurobiological links between social isolation and Alzheimer's disease risk. *Eur J Neurosci*, 56 (2022) 5397.

3 Safiri S, Jolfayi AG, Fazlollahi A, Morsali S, Sarkesh A, Sorkhabi AD, Golabi B, Aletaha R, Asghari KM, Hamidi S, Mousavi SE, Jamalkhani S, Karamzad N, Shamekh A, Mohammadinasab R, Sullman MJM, Şahin F & Kolahi AA, Alzheimer's disease: A comprehensive review of epidemiology, risk factors, symptoms, diagnosis, management, caregiving, advanced treatments and associated challenges. *Front Med*, 11 (2024) 1474043.

4 Yadava U, Negi S & Vishwakarma P, A comparative computational study of the action of various anticonvulsant drugs upon monomeric form of bacterial sodium channel (NavMs), homolog of human voltage-gated sodium channels. *J Mol Liq*, (2026) 129255.

5 Bharadwaj S, Dubey A, Yadava U, Mishra SK, Kang SG & Dwivedi VD, Exploration of natural compounds with anti-SARS-CoV-2 activity via inhibition of SARS-CoV-2 Mpro. *Brief Bioinform*, 22 (2021) 1361.

6 Negi S, Kamboj NK, Babu KG & Yadava U, Investigation of ritonavir analogs antiretroviral natural compounds against SARS-CoV-2 envelope protein. *J Biomol Struct Dyn*, 43 (2025) 874.

7 Negi S & Yadava U, Natural antiretroviral compounds as the inhibitors of the SARS-CoV-2 M protein. *J Mol Liq*, 412 (2024) 125825.

8 Yang PY, Wang YJ, Xi YF, Xin BS, Zhang WQ, Lin B, Yao GD, Lou LL, Huang XX & Song SJ, Targeted discovery of anthranilic acid-based alkaloids with neuroprotective and acetylcholinesterase inhibitory effects from natural indigo plant (*Persicaria tinctoria*) using DeepSAT technology. *Ind Crops Prod*, 226 (2025) 120718.

9 Rizvi SMD, Shakil S & Haneef M, A simple click by click protocol to perform docking: AutoDock 4.2 made easy for non-bioinformaticians. *EXCLI J*, 12 (2013) 830.